Geophysical Research Letters

RESEARCH LETTER
10.1029/2023GL105827

The Dominant Role of the Summer Hemisphere in Subtropical Lower Stratospheric Wave Drag Trends

Marta Abalos[1], William J. Randel[2], and Rolando R. Garcia[2]

[1]Universidad Complutense de Madrid, Madrid, Spain, [2]National Center for Atmospheric Research, Boulder, CO, USA

Key Points:

- Future subtropical trends in lower stratospheric wave drag are strongest in the summer hemisphere, whereas zonal wind trends peak in winter
- The largest changes in transient wave drag due to critical line shift are found in the Southern Hemisphere summer
- The Northern Hemisphere summer trends are mainly due to changes in stationary wave drag linked to stronger and higher deep convection

Correspondence to:
M. Abalos,
mabalosa@ucm.es

Citation:
Abalos, M., Randel, W. J., & Garcia, R. R. (2024). The dominant role of the summer hemisphere in subtropical lower stratospheric wave drag trends. *Geophysical Research Letters*, *51*, e2023GL105827. https://doi.org/10.1029/2023GL105827

Received 4 AUG 2023
Accepted 17 NOV 2023

Author Contributions:
Conceptualization: Marta Abalos
Formal analysis: Marta Abalos
Resources: William J. Randel, Rolando R. Garcia
Writing – original draft: Marta Abalos
Writing – review & editing: Marta Abalos, William J. Randel, Rolando R. Garcia

Abstract It is well established that the shallow branch of the Brewer-Dobson circulation accelerates in a warming climate due to enhanced wave drag in the subtropical lower stratosphere. This has been linked to the strengthening of the upper flanks of the subtropical jets. However, the seasonality of the zonal wind trends, peaking in the winter hemisphere, is opposite to that of the Eliassen-Palm flux convergence trends, peaking in summer. We investigate the seasonality in the wave drag trends and find a different behavior for each hemisphere. The Shepherd and McLandress (2011, https://doi.org/10.1175/2010jas3608.1) mechanism, involving transient wave dissipation at higher levels following the rise of the critical lines, is found to maximize in austral summer. On the other hand, in the Northern Hemisphere the wave drag increase peaks in summer primarily due to the changes in the stationary planetary waves (monsoonal circulations) associated with enhanced deep convection.

Plain Language Summary The Brewer-Dobson circulation, responsible for mass, heat and constituents global transport in the stratosphere, is projected to accelerate in a warming climate. This circulation is driven by the momentum transferred by dissipating waves. We explore the seasonality of trends in wave dissipation in the subtropical lower stratosphere. First, we show that the largest changes in the wave dissipation take place in the summer hemisphere, opposite to the largest changes in the zonal wind, which is known to control wave dissipation conditions. We investigate this apparent contradiction and find that (a) the conditions are particularly favorable for the waves to be affected by the changing wind in summer, due to their spectral characteristics and the structure of the background zonal wind, in particular the proximity of the zero wind line; and (b) in the Northern Hemisphere the changes are primarily associated with stationary waves triggered by enhanced deep convection in a warmer climate.

1. Introduction

The Brewer-Dobson circulation (BDC) is responsible for the zonal mean mass, constituent and heat transport in the stratosphere, and it consists of an advective part, the residual (overturning) circulation, and two-way mixing associated with large-scale quasi-horizontal stirring of air masses following wave breaking (Birner & Bönisch, 2011; Plumb, 2002; Shepherd, 2007). Both transport process are closely associated with wave drag, which is the net transfer of momentum to the mean flow by the eddies as they dissipate. To a large extent, wave dissipation or breaking occurs near the critical lines (Randel & Held, 1991). A critical line is a region where the background zonal wind equals the phase speed of a wave, such that the wave can no longer propagate and is absorbed (or reflected if the absolute vorticity gradient is zero).

It is now a well established result from climate models that the BDC accelerates under increasing greenhouse gas concentrations (Butchart, 2014). In the shallow branch, this is due to enhanced wave drag in the subtropical lower stratosphere (LS), including resolved Rossby and parameterized gravity wave drag, with relative contributions dependent on the model (Abalos et al., 2021; Butchart et al., 2011; Garcia & Randel, 2008; Li et al., 2008; McLandress & Shepherd, 2009). The enhanced drag in the subtropical LS is caused by changes in wave propagation and dissipation conditions due to the strengthened upper flanks of the subtropical jets (Garcia & Randel, 2008). As greenhouse gases increase, the tropical upper troposphere warms and the extratropical stratosphere cools, resulting in a weakening of the (positive poleward) temperature gradient across the subtropical LS. To maintain thermal wind balance, the upper flanks of the subtropical jets strengthen. Shepherd and McLandress (2011) demonstrated that these changes in the winds cause an upward shift of the critical lines for transient waves, which enhances wave drag in that region. In addition, planetary-scale stationary wave drag in

the lower stratosphere is enhanced in a warmer climate due to stronger deep convection in the tropics (Calvo & Garcia, 2009; Deckert & Dameris, 2008; Garny et al., 2011).

Recently, Abalos and de la Cámara (2020) highlighted that the 21st century trends in LS resolved wave drag are notably stronger in the summer hemisphere in one chemistry-climate model. Interestingly, this seasonality is opposite to the seasonality in subtropical jet strengthening (Figures 1a–1d). This opposite seasonality is a robust result across models and is not simply explained by the upward shift of the critical line for transient waves, as one would expect more transient waves penetrating to higher levels as critical lines move higher up. In this paper we investigate the origin of the seasonality in wave drag trends.

2. Data and Methods

For Figure 1 we use output from six models of the Chemistry Climate Model Initiative (CCMI; Eyring et al., 2013): CCSRNIES-MIROC3.2, CMAM, EMAC-L47MA, GEOSCCM, MRI-ESM1r1, and CESM1-WACCM. These models are those that output the zonal-mean acceleration due to the Eliassen-Palm (EP) flux divergence of resolved waves, excluding ACCESS/NIWA because its climatology did not compare well with reanalysis. We used ref-C2 simulations, which follow the RCP6.0 scenario for greenhouse gases and the WMO 2010 scenario for ozone depleting substances. These are fully coupled simulations over 1960–2100, but we only examine the 21st century. A description of the models and simulations is found in Morgenstern et al. (2017).

The rest of the paper uses output from CESM2-WACCM (Gettelman et al., 2019). We use the ref-D2 simulations from 2015 to 2099 carried out for CCMI-2022, which follow an SSP2-4.5 climate change scenario and the ozone depleting substances as specified in the 2022 WMO Ozone Assessment (Chipperfield et al., 2022). All results correspond to the ensemble mean of three members. We evaluate the changes between the beginning and the end of the century, which we refer to as present (2015–2036) and future (2078–2099).

We compute the EP flux divergence as a measure of the wave drag in the Transformed Eulerian Formalism (Andrews et al., 1987)

$$DF = \frac{e^{z/H}}{a\cos\phi}\nabla\cdot\vec{F} = \frac{e^{z/H}}{a\cos\phi}\left(\frac{1}{a\cos\phi}\frac{\partial(F_\phi\cos\phi)}{\partial\phi} + \frac{\partial F_z}{\partial z}\right) \tag{1}$$

where the components of the EP flux are

$$\begin{aligned} F_\phi &= e^{-z/H}a\cos\phi\left(-\overline{u'v'} + \frac{\partial\overline{u}}{\partial z}\frac{\overline{v'T'}}{S}\right) \\ F_z &= e^{-z/H}a\cos\phi\left(\hat{f}\frac{\overline{v'T'}}{S} - \overline{u'w'}\right) \end{aligned} \tag{2}$$

In these equations, bars denote zonal mean and primes deviations from it, a is the Earth's radius, $S = N^2H/R$, where N^2 is the Brunt-Vaisala frequency, $H = 7$ km is the scale height, $R = 287.05\ \mathrm{m^2s^{-2}K^{-1}}$ and $\hat{f} = f - \left(\frac{1}{a\cos\phi}\right)\frac{\partial(\overline{u}\cos\phi)}{\partial z}$. For these calculations we use daily mean output of u, v, T, w to compute the total wave drag, and we use monthly mean output of these fields to compute the stationary wave drag contribution.

In order to examine the longitudinal structure of the stationary wave propagation and dissipation, we compute the three-dimensional stationary wave flux introduced by Plumb (1985):

$$\begin{aligned} F_{S\lambda} &= e^{-z/H}a\cos\phi\left(v'^2 - \frac{1}{2\Omega a\sin 2\phi}\frac{\partial(v'\Phi')}{\partial\lambda}\right) \\ F_{S\phi} &= e^{-z/H}a\cos\phi\left(-u'v' + \frac{1}{2\Omega a\sin 2\phi}\frac{\partial(u'\Phi')}{\partial\lambda}\right) \\ F_{Sz} &= e^{-z/H}a\cos\phi\cdot\frac{f}{S}\left(v'T' - \frac{1}{2\Omega a\sin 2\phi}\frac{\partial(T'\Phi')}{\partial\lambda}\right) \end{aligned} \tag{3}$$

and its divergence

$$DF_S = \frac{e^{z/H}}{a\cos\phi}\nabla\cdot\vec{F_S} = \frac{e^{z/H}}{a\cos\phi}\left(\frac{1}{a\cos\phi}\frac{\partial F_{S\lambda}}{\partial\lambda} + \frac{1}{a\cos\phi}\frac{\partial(F_{S\phi}\cos\phi)}{\partial\phi} + \frac{\partial F_{Sz}}{\partial z}\right) \tag{4}$$

10.1029/2023GL105827

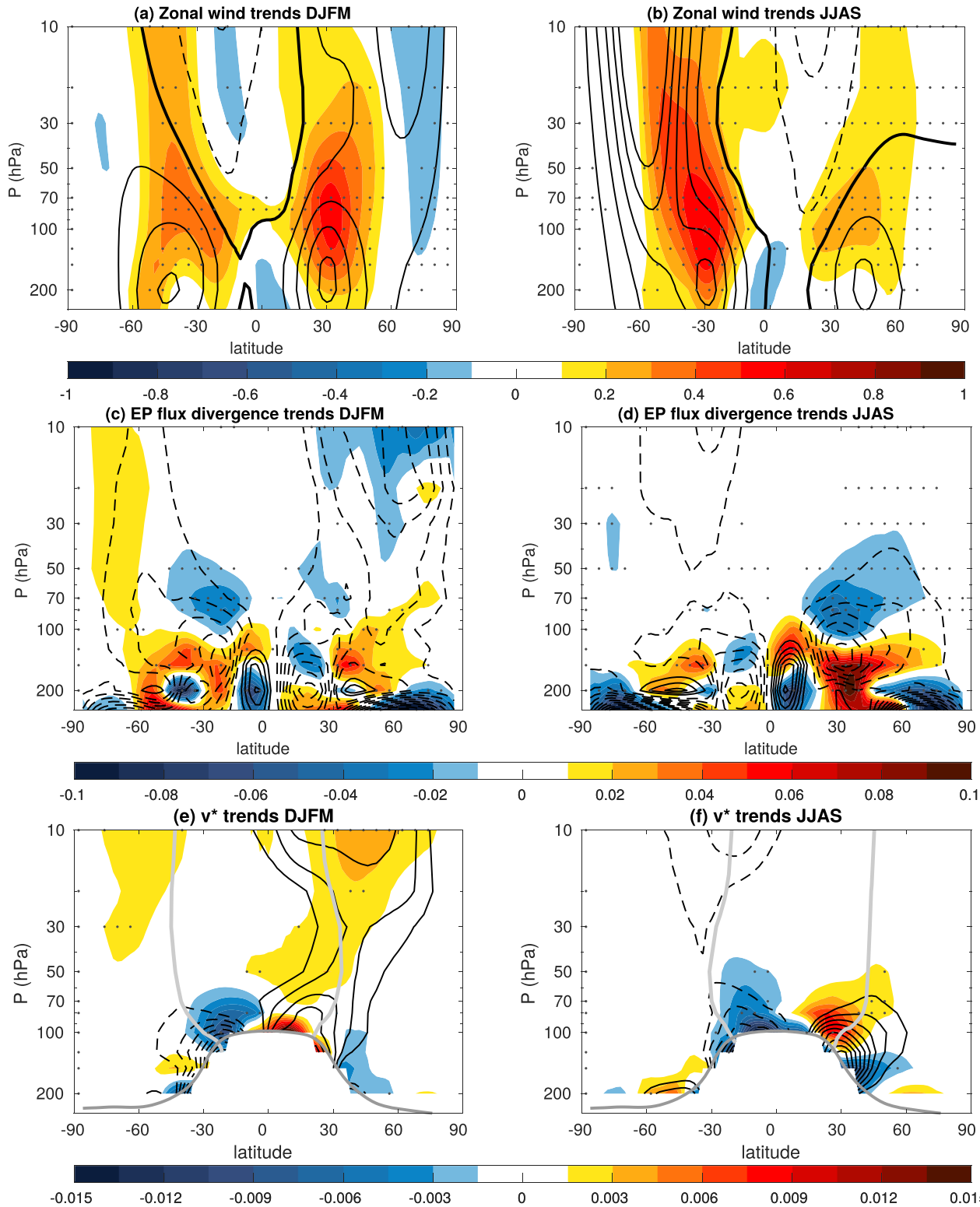

Figure 1. CCMI ref-C2 MMM trends over the 21st century in zonal wind (m s^{-1} $decade^{-1}$, panels (a) and (b)), EP flux divergence (m s^{-1} day^{-1} $decade^{-1}$, panels (c) and (d)) and meridional component of the residual circulation (m s^{-1} $decade^{-1}$, panels (e) and (f) in DJFM (a, c, e) and JJAS (b, d, f)). The black contours show the climatological MMM of the corresponding field, with 10 m s^{-1} (a, b), 0.5 m s^{-1} day^{-1} (c, d) and 0.05 m s^{-1} (e, f) contour interval, with positive (negative) values shown as solid (dashed) lines and the zero contour as a thicker line (only in a). In panels (e) and (f) the tropopause and the turnaround latitudes are shown in dark and light gray, respectively. The dots indicate where all models agree in the sign of the trends.

where all the fields are monthly means and Φ is the geopotential.

We carry out a phase-speed and wavenumber spectral analysis following Randel and Held (1991) and Shepherd and McLandress (2011). For each season (DJFM: December to March, and JJAS: June to September), latitude and height, the space–time cospectrum is calculated for each of the eddy fluxes in Equation 2 as

$$\mathrm{CO}_{\omega,k} = 2\left\langle \mathrm{Re}\left(X_{\omega,k} Y^{*}_{\omega,k}\right)\right\rangle \tag{5}$$

where $X_{\omega,k}$ and $Y_{\omega,k}$ represent the Fourier transform components in time and longitude of the two fields in the eddy flux for a given frequency and wavenumber, and the asterisk indicates the complex conjugate. The angle brackets represent an average over different years. To reduce the effect of spectral leakage due to the finite 120-day time series, we taper the series with a Hanning window. The cospectrum is then smoothed with a 3 point running mean in frequency and expressed as a function of phase speed $c = \omega/k$ ensuring the conservation of total power $\mathrm{CO}_{c,k} = k\mathrm{CO}_{\omega,k}$. The results are then summed over wavenumbers and shown as a function of latitude or altitude.

3. Results

Figure 1 shows the CCMI multi-model mean (MMM) trends over the 21st century in zonal wind and EP flux divergence (DF in the rest of the paper), highlighting the opposite seasonality of the trends in the two fields in the subtropical LS. Although this opposite seasonality is a consistent result across all the models, it has not been discussed previously and is the focus of the present paper. We note that the positive DF trends in the SH high latitudes in DJFM are due to stratospheric ozone recovery (McLandress et al., 2010; Polvani et al., 2018), while the trends of interest to this study (LS subtropics) are due to greenhouse gas increases. Consistent with the stronger resolved drag increase in summer, the increase in the poleward outflow of the shallow branch at the turnaround latitudes is larger in the summer hemisphere, especially in the NH (Figures 1e and 1f). On the other hand, the seasonality in tropical upwelling trends is highly variable across models (not shown) because it is additionally influenced by resolved and gravity wave drag at higher levels from both hemispheres, consistent with Butchart et al. (2011).

In order to understand the mechanism behind the seasonality in the DF trends, we focus our attention on the CESM2-WACCM simulations for the rest of the paper. Figure 2 shows the difference future minus present in the total (resolved) DF field (a, b), and contributions from stationary waves (c, d), transient waves (e, f) and parameterized gravity wave drag (GWD; g and h). The GWD is dominated by the orographic component, but we show the total GWD including frontal and convective parameterizations as well. The transient wave contribution is obtained as the difference of the total resolved wave drag minus the stationary contribution. The top panels in Figure 2 are consistent with the bottom panels in Figure 1, in that the summer hemisphere drag trends in the subtropical LS are much stronger than in winter. There are dipole-like patterns in the summer hemisphere subtropics, with divergence in the upper troposphere (UT) and convergence in the LS. The pattern is stronger in JJAS than in DJFM, and this is not due to the counteracting effect of the ozone recovery, as that is limited to latitudes south of ∼50 S according to sensitivity simulations (not shown). The dipolar patterns suggest an upward shift of the climatological wave drag, with reduced drag in the lower part of the climatological convergence regions and enhanced drag in the upper part. Indeed, the pattern largely disappears in tropopause-relative coordinates, consistent with the expansion of the troposphere under global warming (Oberländer-Hayn et al., 2016). It is interesting to note that the climatological LS EP flux convergence regions are stronger in the summer than in the winter hemisphere, and thus the upward shift of those regions will result in stronger trends in the summer hemisphere, as observed.

It is clear that the Northern Hemisphere (NH) JJAS trends are dominated by stationary waves, while the Southern Hemisphere (SH) DJFM trends are dominated by transient waves, as the stationary drag trends are much smaller (though not negligible). The GWD plays an important role in the NH winter. Note that it maximizes in the region of near zero changes in resolved drag, consistent with the compensation mechanism (Sigmond & Shepherd, 2014). The contributions from different waves to the residual circulation (TEM) streamfunction computed using downward control (Haynes et al., 1991) are shown in Figures 2i and 2j. We note that the primary role of stationary waves in the NH summer is consistent across CCMI models (not shown). In light of the results in Figure 2, we next focus on the transient wave drag spectrum in DJFM and investigate the origin of the stationary wave contribution in JJAS.

10.1029/2023GL105827

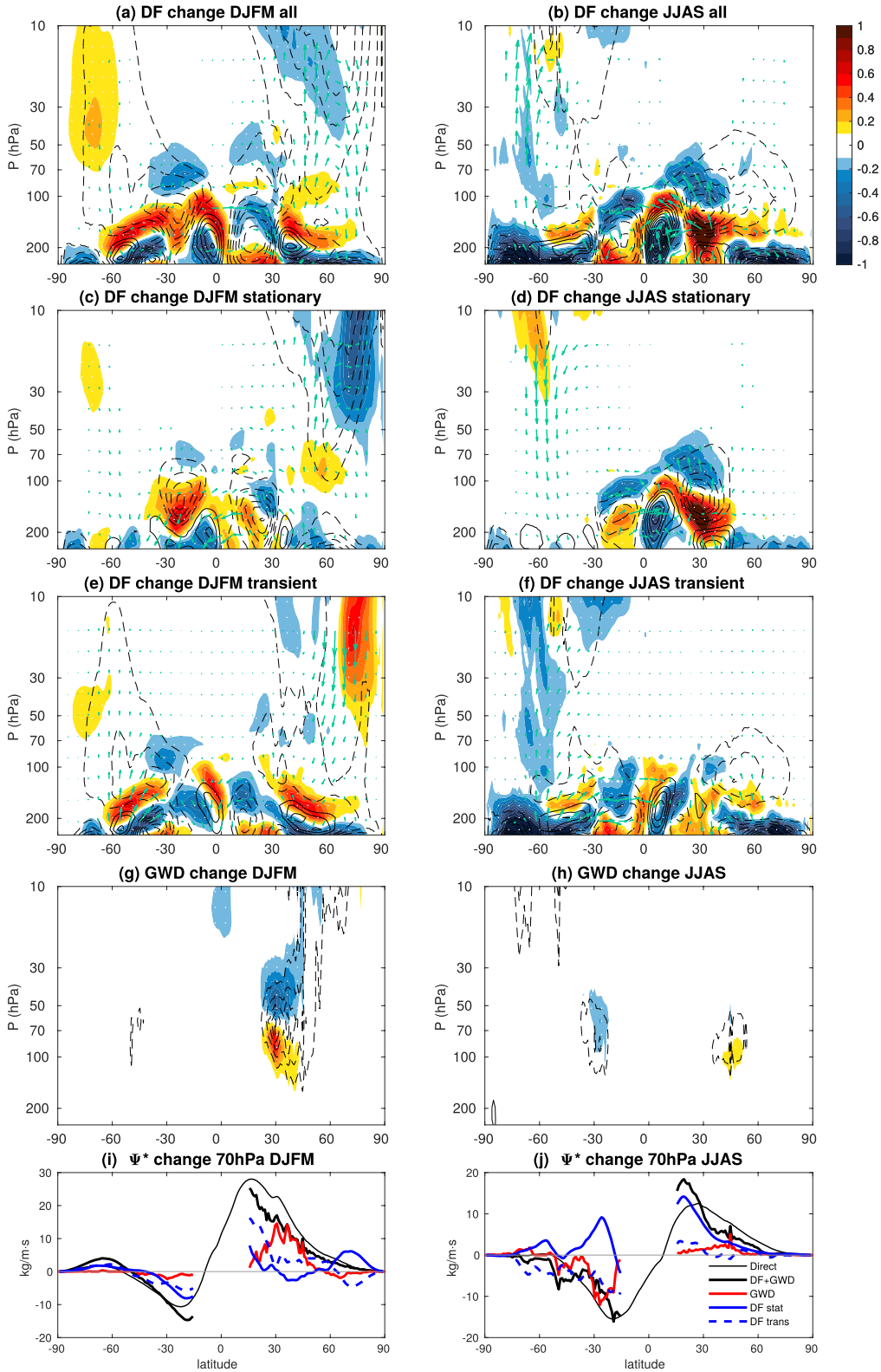

Figure 2. Future minus present total DF (a, b), stationary DF (c, d), transient DF (e, f) and GWD (g, h) from CESM2-WACCM ref-D2 (in m s^{-1} day^{-1}). Left: DJFM, right: JJAS. Black contours: climatological corresponding drag, 0.5 m s^{-1} day^{-1} contour interval; positive: solid, negative: dashed, zero: omitted. Arrows in (a)–(f): EP flux components scaled arbitrarily (vertical component multiplied by 500). White dots: statistically significant changes with a Student *t* test at the 95% confidence level. (i, j): Change in TEM streamfunction and contribution from each forcing calculated by downward control.

Figure 3a shows the latitudinal distribution of the DF cospectrum and its trends in DJFM in the LS. Both hemispheres show climatological DF convergence that peaks in the subtropics and is larger in the SH. There is a clear interhemispheric asymmetry in the wave drag trends. In the SH there is a strong wave drag increase that extends from 0 to 40 S, coinciding with the equatorward shift of the critical lines (phase speeds between 0 and 20 m/s). Figure 3b shows that this constitutes a reinforcement of the upper part of the climatological wave drag (about 100–50 hPa), which is due to enhanced upward and equatorward propagation of waves into that region following the shift in the critical line, as seen from the F_ϕ and F_z cospectra (not shown). This reinforcement is associated with both planetary and synoptic waves, with the former contributing about 2/3 (Figures 3d, 3e, 3g, and 3h), while synoptic waves play a larger role in the deep tropics (Figure 3g).

In the NH in contrast, Figure 3a shows a dipole between 20 and 40 N, with enhanced DF convergence over the phase speeds where the critical line is shifting to higher values (around 25 m/s), and reduced DF convergence at lower phase speeds (around 10 m/s). The enhanced wave drag is due to planetary scale waves, while the reduced drag is mainly linked to synoptic waves (Figures 3d and 3g). Figure 3c further illustrates this behavior: there is a dipole in the total drag, suggesting enhanced wave propagation to higher levels (shown also by the upward pointing arrows in Figure 2a), following the upward shift in the critical lines. Nevertheless, the dipole is largely split into planetary and synoptic waves. The enhanced drag near the critical line is mainly due to planetary waves, while the reduction of wave drag for lower phase speeds is mainly due to synoptic waves. These results are consistent with Shepherd and McLandress (2011), although that study only considers the latitude of 30 N. By considering the latitudinal average over 20–40 N we include a region of positive DF change lying on the upper part of the positive climatological DF at 30–60 N between 200 and 100 hPa in Figure 2e, linked to the synoptic waves with phase speeds lower than 20 m/s. This likely reflects an upward shift in the region of transient synoptic wave generation poleward of the jet core. When summing over all phase speeds, the positive trends at lower phase speeds partly cancel out the negative trends at higher phase speeds and the net drag increase is smaller in the NH than in the SH. In summary, the SH summer trends are larger than their NH counterpart because (a) the climatological drag is larger, and (b) both planetary and synoptic waves contribute, without cancellation between high and low phase speed waves. In JJAS the transients play a minor role, with enhanced drag in the easterly phase speeds between 0 and 30 N (not shown).

In order to investigate the origin of the stationary waves that dominate the NH JJAS trends, Figure 4a shows the change in geopotential height anomalies together with the change in latent heating from convection at 250 hPa, where it is most pronounced. There is a marked wave-1 pattern in the geopotential height zonal anomalies in the subtropics, with higher altitudes on the eastern flank of the Asian monsoon anticyclone extending into the Pacific, and lower altitudes centered over western North America. The positive anomalies are located over a region of a ∼20% increase in latent heat released by enhanced deep convection in the Asian monsoon. The longitude-latitude pattern of stronger convective activity mirrors the climatology (not shown), and the vertical structure reveals an upward shift and intensification of the deep convection (Figure 4b).

Figure 4c shows the change in the Plumb flux for stationary waves averaged over the subtropical region as a function of altitude and longitude. The enhanced convection in the Asian monsoon region results in a stronger wave source (Plumb flux divergence) centered at about 110 E and near 120 hPa from which stationary waves emanate upward (and downward) and dissipate in the LS. This region makes the largest contribution to the strong EP flux divergence seen in Figure 2c in the NH subtropical UT. Comparing the trends to the climatology patterns again suggests a strengthening and upward shift in wave generation, upward propagation and dissipation in the LS (Figure 4d). The enhanced convection over South America and Africa also produce enhanced wave generation and dissipation dipoles, although the waves dissipate at lower levels than in the Asian monsoon region. Overall, Figure 4 suggests that the enhanced wave drag in boreal summer is associated with changes in stationary planetary waves generated by convection rather than by changes in transient wave propagation. The transient wave drag in JJAS is enhanced in the region of easterlies between 0 and 20N (not shown), but this makes a smaller contribution than the stationary waves (compare Figures 2d and 2f).

4. Conclusions and Discussion

Shepherd and McLandress (2011) showed that the prevailing mechanism for the acceleration of the residual circulation in the LS is the upward shift in the region of dissipation of transient waves (both planetary and synoptic) and orographic gravity waves, enabled by the upward displacement in the critical lines associated with

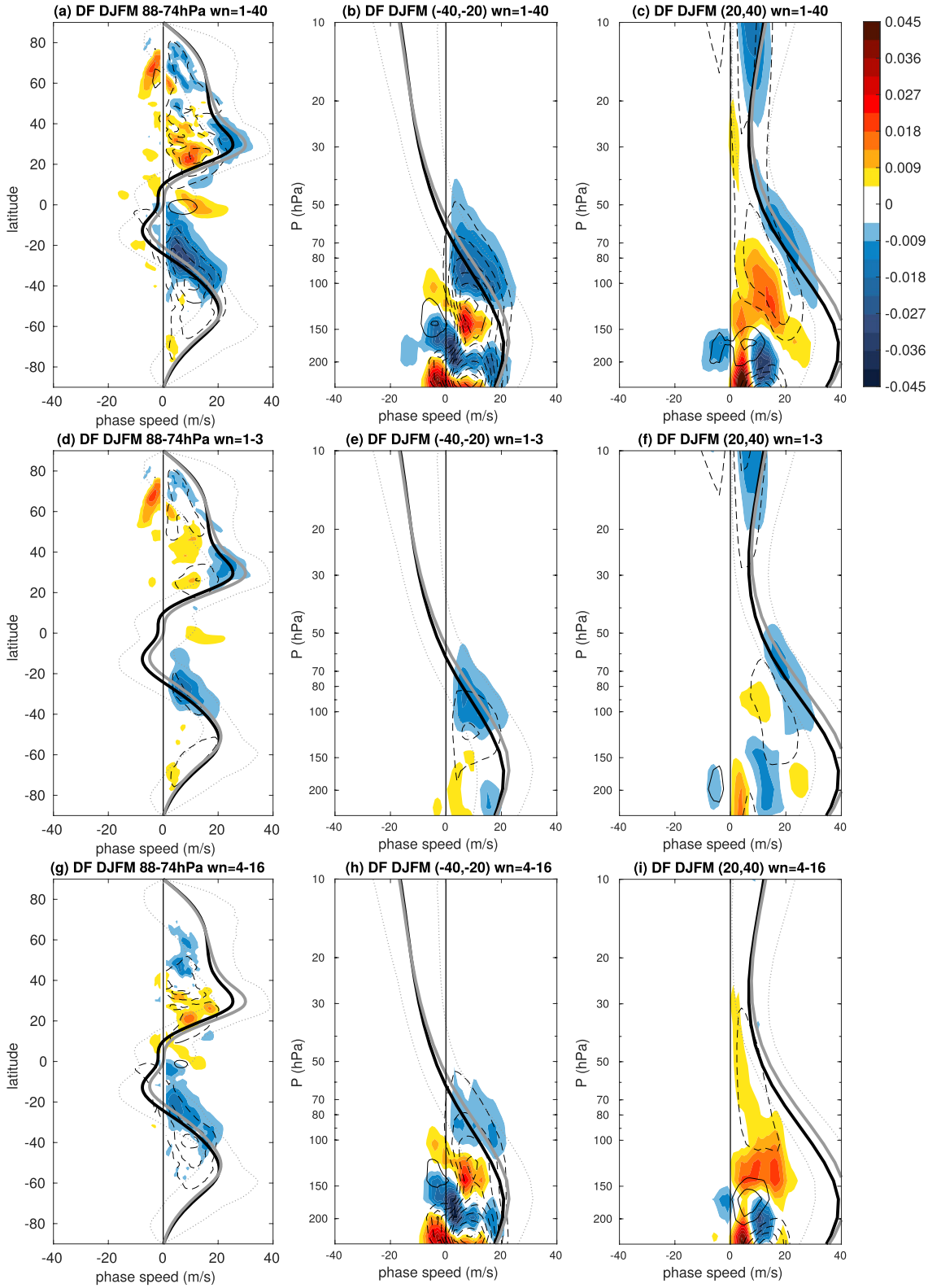

Figure 3. Future minus present change (shading) in the DJFM wave drag (DF) cospectrum for wavenumbers 1–40 as a function of latitude averaged over the levels 88–74 hPa (a, d, g) and as a function of height averaged over the latitudes 20–40 S (b, e, h) and 20–40 N (c, f, i) in units of m s^{-1} day^{-1}. Panels (a–c): wavenumbers 1–40, d–f: 1–3, e–i: 4–16. The thin black contours show the climatological DF cospectrum for the present (solid positive, dashed negative). Thick black (gray) solid line: zonal mean wind climatology in the present (future). Dotted lines: range of variability in the zonal wind in the future.

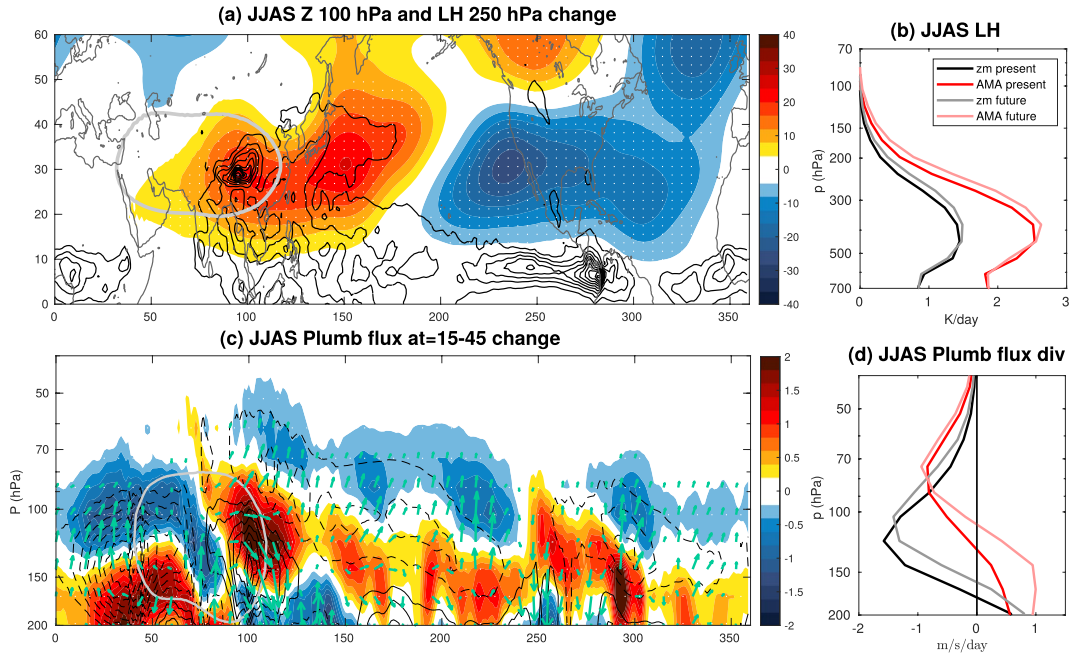

Figure 4. (a, c): Future minus present change in JJAS (a) geopotential height zonal anomalies at 100 hPa (shading, in m) and latent heating due to convection at 250 hPa (black contours, contour interval 0.25 Kday^{-1}, all are positive values) and (c) Plumb flux divergence (shading, in m s^{-1} day^{-1}) and components in the longitude-altitude plane averaged over 15–45 N (F_x and F_z arrows). Black contours: present climatology of the convergence (solid positive, dashed negative, contour interval: 1 m s^{-1} day^{-1}). The green contour in both panels depicts the 90 m level of climatological geopotential height zonal anomaly to identify the Asian monsoon anticyclone. White dots as in Figure 3. (b, d): Latent heat due to convection (b) and Plumb flux divergence (d) in the present and future periods averaged over latitudes 10–45 N for the zonal mean (black: present, gray: future) and the Asian monsoon region (40–120 E, red: present, light red: future).

strengthening of the upper flank of the jets. Previous studies had shown enhanced stationary wave activity in the tropical LS linked to strengthened deep convection (Calvo & Garcia, 2009; Deckert & Dameris, 2008; Garny et al., 2011). In this study we revisit the mechanisms responsible for the wave drag trends in the LS with a focus on the seasonality, motivated by the fact that the resolved wave drag increases more in the summer hemisphere, contrary to the behavior of the zonal wind, which experiences a larger change in the winter hemisphere.

We find that the two factors determine the seasonality, and each factor is most relevant in a given season. First, the climatological transient EP flux convergence is largest in the summer hemisphere LS, consistent with a lower zero wind line in this season and background winds closer to the phase-speeds of the transient waves, which are below 20 m/s in both summer and winter. Consequently, the acceleration of the zonal wind has a larger effect in summer, when the waves are closer to their critical lines, while in winter a large fraction of the waves can propagate farther up into the stratosphere. This factor is most important for austral summer. In boreal summer, changes in the stationary waves associated with the upward shift of latent heat release by deep convection play a dominant role in the enhanced EP flux convergence. The enhanced convection may have a larger impact in boreal than in austral summer because the deep convective activity extends farther into the subtropics, due to the land-sea distribution and orography (Himalayas).

Enhanced deep convection over the Asian monsoon region is a key contributor to the stationary wave changes in CESM2-WACCM, but it is important to note that there is a large uncertainty in response of the Asian monsoon to greenhouse gas increases (Lee & Zhou, 2021). Shaw and Voigt (2015) argue that the large intermodel spread in the Asian monsoon circulation trends is explained by different compensation between counteracting effects of increased heating over land and over ocean. The pattern observed in Figure 4 suggests that in CESM2-WACCM the first mechanism dominates. Consistent with Shaw and Voigt (2015), geopotential trend patterns in other models are somewhat different than those in Figure 4a (not shown). Nevertheless, the stationary wave drag dominates boreal summer LS across models. The details of future changes in deep convection are likely model dependent, because they are controlled by parameterizations and may also depend on the distribution of surface

warming. Further studies are needed to evaluate the specific contributors to enhanced JJAS stationary wave drag in other models.

The seasonality of trends in wave drag affects the lower branch of the residual circulation. While all the analyzed CCMI models show stronger wave drag trends in the summer hemisphere, the relative strength between the NH and SH summer drag is model-dependent. As a result of differences in relative contributions from the two hemispheres, and in resolved and parameterized waves at higher levels, the seasonality of the trends in upwelling is different in each model (not shown). On the other hand, we find that the shallow branch poleward outflow is strongest in the summer, especially in the NH.

The upward shift in the deep convection is closely coupled to the upward shift in the tropopause, both reflecting the fact that the UT becomes less stable, and thus the troposphere becomes convectively unstable throughout a greater depth, as greenhouse gases increase. Consistently, the wave drag trends are much smaller when calculated in tropopause-relative coordinates, and likewise for the residual circulation changes (Abalos et al., 2017; Oberländer-Hayn et al., 2016). Finally, it is worth noting that the cold pole bias present in models leads to a substantially higher zero wind line than observed in austral summer, which could hamper the ability to represent wave drag trends.

Data Availability Statement

The CCMI output used in this study was downloaded from https://data.ceda.ac.uk/badc/wcrp-ccmi/data/CCMI-1/. The CESM2-WACCM6 output is available at https://data.ceda.ac.uk/badc/ccmi/data/post-cmip6/ccmi-2022/.

Acknowledgments
The authors acknowledge the reviewers for insightful comments. MA acknowledges funding from the Spanish National project RecO3very (ref: PID2021-124772OB-I00) and the Atmospheric Chemistry Observations and Modeling Visitor Program (NCAR). We acknowledge high-performance computing and storage support from Cheyenne (https://doi.org/10.5065/D6RX99HX) provided by NCAR's Computational and Information Systems Laboratory, sponsored by the National Science Foundation. We are thankful to the ISSI-TWIST (Tropical Width Impacts On The Stratosphere), Isla Simpson and Alvaro de la Cámara for helpful discussions.

References

Abalos, M., Calvo, N., Benito-Barca, S., Garny, H., Hardiman, S. C., Lin, P., et al. (2021). The Brewer–Dobson circulation in CMIP6. *Atmospheric Chemistry and Physics*, *21*(17), 13571–13591. https://doi.org/10.5194/acp-21-13571-2021

Abalos, M., & de la Cámara, A. (2020). Twenty-first century trends in mixing barriers and eddy transport in the lower stratosphere. *Geophysical Research Letters*, *47*(21), e2020GL089548. https://doi.org/10.1029/2020GL089548

Abalos, M., Randel, W. J., Kinnison, D. E., & Garcia, R. R. (2017). Using the artificial tracer e90 to examine present and future UTLS tracer transport in WACCM. *Journal of the Atmospheric Sciences*, *74*(10), 3383–3403. https://doi.org/10.1175/JAS-D-17-0135.1

Andrews, D. G., Holton, J., & Leovy, C. B. (1987). *Middle atmosphere dynamics*. Academic Press.

Birner, T., & Bönisch, H. (2011). Residual circulation trajectories and transit times into the extratropical lowermost stratosphere. *Atmospheric Chemistry and Physics*, *11*(2), 817–827. https://doi.org/10.5194/acp-11-817-2011

Butchart, N. (2014). The Brewer-Dobson circulation. *Reviews of Geophysics*, *52*(2), 157–184. https://doi.org/10.1002/2013RG000448

Butchart, N., Charlton-Perez, A. J., Cionni, I., Hardiman, S. C., Haynes, P. H., Krüger, K., et al. (2011). Multimodel climate and variability of the stratosphere. *Journal of Geophysical Research*, *116*(D5), D05102. https://doi.org/10.1029/2010JD014995

Calvo, N., & Garcia, R. R. (2009). Wave forcing of the tropical upwelling in the lower stratosphere under increasing concentrations of greenhouse gases. *Journal of the Atmospheric Sciences*, *66*(10), 3184–3196. https://doi.org/10.1175/2009JAS3085.1

Chipperfield, M. P., Santee, M. L., Alexander, S. P., de Laat, A. T. J., Kinnison, D. E., Kuttippurath, J., et al. (2022). Polar stratospheric ozone: Past, present, and future. In *WMO*. In *Scientific assessment of ozone depletion: 2022, GAW Report No. 278* (p. 509). (chap. 4).

Deckert, R., & Dameris, M. (2008). Higher tropical SSTs strengthen the tropical upwelling via deep convection. *Geophysical Research Letters*, *35*(10), L10813. https://doi.org/10.1029/2008GL033719

Eyring, V., Lamarque, J.-F., Hess, P., Arfeuille, F., Bowman, K., Chipperfield, M. P., et al. (2013). Overview of IGAC/SPARC chemistry-climate model initiative (CCMI) community simulations in support of upcoming ozone and climate assessments. *SPARC Newsletter*, (40), 48–66.

Garcia, R. R., & Randel, W. J. (2008). Acceleration of the Brewer–Dobson circulation due to increases in greenhouse gases. *Journal of the Atmospheric Sciences*, *65*(8), 2731–2739. https://doi.org/10.1175/2008JAS2712.1

Garny, H., Dameris, M., Randel, W., Bodeker, G. E., & Deckert, R. (2011). Dynamically forced increase of tropical upwelling in the lower stratosphere. *Journal of the Atmospheric Sciences*, *68*(6), 1214–1233. https://doi.org/10.1175/2011JAS3701.1

Gettelman, A., Mills, M. J., Kinnison, D. E., Garcia, R. R., Smith, A. K., Marsh, D. R., et al. (2019). The whole atmosphere community climate model version 6 (WACCM6). *Journal of Geophysical Research: Atmospheres*, *124*(23), 12380–12403. https://doi.org/10.1029/2019JD030943

Haynes, P. H., Marks, C. J., McIntyre, M. E., Shepherd, T. G., & Shine, K. P. (1991). On the "downward control" of extratropical diabatic circulations by eddy-induced mean zonal forces. *Journal of the Atmospheric Sciences*, *48*(4), 651–678. https://doi.org/10.1175/1520-0469(1991)048⟨0651:OTCOED⟩2.0.CO;2

Lee, J.-Y., Marotzke, J., Bala, G., Cao, L., Corti, S., Dunne, J. P., et al. (2021). Future global climate: Scenario-based projections and near-term information. In *Climate change 2021: The physical science basis. Contribution of working group I to the sixth assessment report of the intergovernmental panel on climate change*. Cambridge University Press. (chap. 4). https://doi.org/10.1017/9781009157896.006

Li, F., Austin, J., & Wilson, J. (2008). The strength of the Brewer-Dobson circulation in a changing climate: Coupled chemistry-climate model simulations. *Journal of Climate*, *21*(1), 40–57. https://doi.org/10.1175/2007JCLI1663.1

McLandress, C., Jonsson, A. I., Plummer, D. A., Reader, M. C., Scinocca, J. F., & Shepherd, T. G. (2010). Separating the dynamical effects of climate change and ozone depletion. Part I: Southern Hemisphere stratosphere. *Journal of Climate*, *23*(18), 5002–5020. https://doi.org/10.1175/2010JCLI3586.1

McLandress, C., & Shepherd, T. G. (2009). Simulated anthropogenic changes in the Brewer-Dobson circulation, including its extension to high latitudes. *Journal of Climate*, *22*(6), 1516–1540. https://doi.org/10.1175/2008JCLI2679.1

Morgenstern, O., Hegglin, M. I., Rozanov, E., O'Connor, F. M., Abraham, N. L., Akiyoshi, H., et al. (2017). Review of the global models used within phase 1 of the chemistry–climate model initiative (CCMI). *Geoscientific Model Development*, *10*(2), 639–671. https://doi.org/10.5194/gmd-10-639-2017

Oberländer-Hayn, S., Gerber, E. P., Abalichin, J., Akiyoshi, H., Kerschbaumer, A., Kubin, A., et al. (2016). Is the Brewer-Dobson circulation increasing or moving upward? *Geophysical Research Letters*, *43*(4), 1772–1779. https://doi.org/10.1002/2015GL067545

Plumb, R. A. (1985). On the three-dimensional propagation of stationary waves. *Journal of the Atmospheric Sciences*, *42*(3), 217–229. https://doi.org/10.1175/1520-0469(1985)042⟨0217:OTTDPO⟩2.0.CO;2

Plumb, R. A. (2002). Stratospheric transport. *Journal of the Meteorological Society of Japan*, *80*(4B), 793–809. https://doi.org/10.2151/jmsj.80.793

Polvani, L. M., Abalos, M., Garcia, R., Kinnison, D., & Randel, W. J. (2018). Significant weakening of Brewer-Dobson circulation trends over the 21st century as a consequence of the Montreal protocol. *Geophysical Research Letters*, *45*(1), 401–409. https://doi.org/10.1002/2017GL075345

Randel, W. J., & Held, I. (1991). Phase speed spectra of transient eddy fluxes and critical layer absorption. *Journal of the Atmospheric Sciences*, *48*(5), 688–697. https://doi.org/10.1175/1520-0469(1991)048<0688:pssote>2.0.co;2

Shaw, T., & Voigt, A. (2015). Tug of war on summertime circulation between radiative forcing and sea surface warming. *Nature Geoscience*, *8*(8), 560–566. https://doi.org/10.1038/ngeo2449

Shepherd, T. G. (2007). Transport in the middle atmosphere. *Journal of the Meteorological Society of Japan. Series II*, *85B*(0), 165–191. https://doi.org/10.2151/jmsj.85B.165

Shepherd, T. G., & McLandress, C. (2011). A robust mechanism for strengthening of the Brewer–Dobson circulation in response to climate change: Critical-layer control of subtropical wave breaking. *Journal of the Atmospheric Sciences*, *68*(4), 784–797. https://doi.org/10.1175/2010JAS3608.1

Sigmond, M., & Shepherd, T. G. (2014). Compensation between resolved wave driving and parameterized orographic gravity wave driving of the Brewer–Dobson circulation and its response to climate change. *Journal of Climate*, *27*(14), 5601–5610. https://doi.org/10.1175/JCLI-D-13-00644.1